Groundwater flow through anisotropic fault zones in multiaquifer systems

E. I. Anderson[1] and M. Bakker[2]

Received 15 February 2008; revised 13 July 2008; accepted 8 September 2008; published 29 November 2008.

[1] Vertical faults through the shallow crust are commonly believed to act as either barriers to horizontal groundwater flow normal to the fault, conduits to horizontal flow tangential to the fault, or a combination of both. In addition, enhanced vertical permeability has been identified as a common feature. We investigate the effects of vertical anisotropy of a fault zone on the distribution of hydraulic head within the fault, using an analytic solution. We conclude that anisotropy ratios greater than 100 result in nearly hydrostatic conditions within the fault zone, despite the existence of significant vertical flow rates. Under these conditions, the Dupuit approximation is adequate for predicting the flow from one side of the fault to the other. We then present explicit analytical solutions to problems of steady groundwater flow in a multiaquifer system cut by a single vertical fault. The fault is linear and of negligible width, is infinite in length, and acts as a conduit for vertical fluid flow. The fault may act as a leaky barrier to horizontal flow normal to the fault, as a conduit to horizontal flow tangential to the fault, or a combination of both. Examples are presented that highlight the effects of enhanced vertical permeability of a fault on aquifer interaction in a multiaquifer system. Particle tracking is used to investigate the effects of the fault on pathlines.

Citation: Anderson, E. I., and M. Bakker (2008), Groundwater flow through anisotropic fault zones in multiaquifer systems, *Water Resour. Res.*, *44*, W11433, doi:10.1029/2008WR006925.

1. Introduction

[2] The bulk hydrologic properties of fault zones are believed to be highly anisotropic. Vertical or near-vertical faults are commonly described as being either conduits for horizontal flow along the fault, barriers to horizontal flow across the fault, or a combination of both. In addition, faults often are believed to act as conduits for vertical flow [*Bredehoeft et al.*, 1992; *Bense et al.*, 2003a, 2003b; *Maslia and Prowell*, 1990] because of an enhanced vertical permeability within the fault plane.

[3] *Bredehoeft et al.* [1992] adopted a fault model with enhanced vertical permeability and low normal permeability to explain the nearly hydrostatic conditions observed throughout the deep, multiaquifer system of the Big Horn Basin, Montana. Using a finite difference model of groundwater flow, the faults were modeled as anisotropic features with large vertical hydraulic conductivities, up to three orders of magnitude larger than the hydraulic conductivities of the adjacent aquifers and up to seven orders of magnitude larger than the horizontal hydraulic conductivity of the fault. The model results showed nearly hydrostatic conditions over the depth of the faults. The faults in the Basin also act as barriers to horizontal flow; the hydraulic head is observed to drop significantly across individual faults.

[4] In addition to equilibrating heads in multiaquifer systems, a fault may provide a pathway for the rapid transport of contaminants both laterally along the fault and vertically between otherwise isolated aquifer layers. As a consequence, faults can have great influence on transport processes in the subsurface. *Maslia and Prowell* [1990] attribute chloride contamination in the Upper Floridan aquifer in Brunswick, Georgia to interaction with underlying aquifers through enhanced vertical flow in fault zones. *Bense et al.* [2003a, 2003b] inferred enhanced vertical permeability in faults in the Roer Valley Rift System in the Netherlands based on groundwater temperature data and the location of springs. Many of the faults studied by Bense et al. are also characterized as strong barriers to horizontal flow normal to the faults.

[5] *Bense and Person* [2006] discussed the combined barrier conduit effects of the Baton Rouge Fault which cuts through a thick sequence of siliciclastic sediments in south Louisiana. A large change in hydraulic head is observed across the fault, suggesting low permeabilities normal to the fault plane; isotope and geochemical data, however, suggest large vertical permeabilities within the fault plane. Bense and Person conducted a parametric study using two-dimensional, vertical plane numerical models of steady groundwater flow in a faulted multiaquifer system. Fault anisotropy values of 10^2 to 10^3 (vertical fault permeability/normal fault permeability) were assigned in the models.

[6] Several researchers have attempted to measure or predict the anisotropic, bulk permeability field associated with the combined fault damage and core zones. *Antonellini and Aydin* [1994] measured the permeability of the damage

[1]SEH Inc., Appleton, Wisconsin, USA.
[2]Water Resources Section, Faculty of Civil Engineering and Geosciences, Delft University of Technology, Delft, Netherlands.

0043-1397/08/2008WR006925$09.00

zone and core zone of sandstone outcrops using minipermeameters and conclude that both fault features are distinctly aniosotropic; estimates of the bulk permeability of the fault indicate an anisotropy ratio of 10^2. More recently, several researchers have used fracture flow models based on detailed fracture measurements at fault outcrops to predict, through numerical simulation, properties of the upscaled permeability tensors associated with the fault zones. *Caine and Forester* [1999] simulate fracture networks in low permeability rocks and predict anisotropy ratios ranging from 10^0 to 10^5. *Jourde et al.* [2002] report studies of fracture networks in a simulated eolian sandstone and conclude that anisotropy ratios range from 10^2 to 10^3. *Flodin et al.* [2004] report similar values in faulted sandstone. It is a common conclusion of these studies that the bulk vertical permeability of a fault can be several orders of magnitude higher than the horizontal permeabilities normal and tangential to the fault.

[7] Here we begin by investigating the effects on groundwater flow of vertical anisotropy in an idealized fault. Our results confirm the conclusion of *Bredehoeft et al.* [1992] that high anisotropy ratios can result in nearly hydrostatic conditions within the fault. We then present an analytical framework and explicit analytical solutions for modeling steady groundwater flow in a faulted multiaquifer system. The fault is modeled as a linear feature of negligible width cutting vertically through an aquifer system, with an arbitrary number of aquifer layers on both sides of the fault. Within the fault, we adopt the Dupuit approximation and allow concentrated vertical flow without head loss [*Polubarinova-Kochina*, 1962; *Strack*, 1989].

[8] Our work follows the approach of *Hunt and Curtis* [1989], *Maas* [2000], and *Bakker* [2006]. *Hunt and Curtis* [1989] presented an analytical solution for flow in a multiaquifer system in which the leaky aquitards end abruptly resulting in a single, unlayered aquifer. Hunt and Curtis used the concept of a single comprehensive discharge potential [*Strack*, 1989] to describe the comprehensive discharge vector: the sum of the discharge vectors over the depth of the entire multiaquifer system. The solution to the comprehensive problem provided the boundary conditions for the multiaquifer flow problem. *Maas* [2000] presented the solution for a faulted multiaquifer system where the fault is represented only as a vertical shortcut between the aquifers. Maas also used the comprehensive potential and the solution to the comprehensive problem to provide boundary conditions for the multiaquifer flow solution. Maas's solution allows for multiaquifer systems with differing properties to lie on either side of the fault. *Bakker* [2006] used analytic elements to extend the Maas solution to polygonal multiaquifer domains embedded in a single aquifer. Both the solutions of *Hunt and Curtis* [1989] and of *Maas* [2000] are special cases of the solution presented here.

[9] The work presented here was motivated by difficulties encountered performing regional-scale modeling studies of aquifers containing faults or fault zones [e.g., *Bakker et al.*, 1999]. Two problems were commonly encountered when modeling faults: first, characterization of the hydraulic properties of faults is difficult and identifying fault properties through hypothesis testing by comparing model results to observed head patterns is not possible, without extensive field data [*Anderson*, 2006]; second, faults are relatively thin, linear features over which large, three-dimensional property changes can occur. Numerical models, such as the one presented by *Bredehoeft et al.* [1992], commonly represent faults with a single cell width. In cases with large vertical anisotropy, combined with a high resistance to normal flow, it is unlikely that the models can accurately predict three-dimensional discharges or pathlines through the fault. Numerical models that discretize the fault zone finely to obtain accurate discharges and pathlines within the fault, such as those presented by *Bense and Person* [2006] are limited by computational demands to two dimensions.

[10] The analytical model and results presented here have three purposes: first, we gain insight and develop understanding of advective transport within and across highly anisotropic faults in multiaquifer systems. Second, we provide the explicit solution to a complex, three-dimensional problem with thin zones of highly anisotropic properties, which may be used to validate numerical codes, such as those developed by *Bense and Person* [2006]. Finally, the model itself may be used to design and analyze steady state field tests aimed at assessing fault properties.

2. Vertical Flow in an Anisotropic Fault

[11] We begin by investigating the effects of vertical anisotropy on flow and head distributions within a fault. We consider a single aquifer cut by a vertical fault and offset across the fault zone as illustrated in Figure 1a. Figure 1b illustrates the boundary value problem developed from the conceptual model shown in Figure 1a. The problem lies in the yz plane, where the z axis points vertically upward. We model only the fault domain; we represent the steady flow from the aquifer to the fault by specifying the normal component of specific discharge, N [L/T], to be constant over the depth of the aquifer, while the remaining boundaries are impermeable.

[12] We present an analytical solution and results for the specific geometry shown in Figure 1b where the aquifer has a thickness H, the two sides are offset by a vertical distance of $2H$, and the width of the fault is specified as $w = H/2$. The parameter A is the fault anisotropy ratio

$$A = \frac{k_z}{k_y} \tag{1}$$

and k_z and k_y are the vertical and horizontal hydraulic conductivities of the fault, respectively. The solution to this problem is presented here without derivation. The hydraulic head, $h(y, z)$, and stream function, $\Psi(y, z)$, may be obtained from the real and imaginary parts, respectively, of a single complex function, Ω, as

$$h(y,z) = \Re\{\Omega(y,z)\}/\left(\sqrt{A}k_y\right) \tag{2}$$

$$\Psi(y,z) = \Im\{\Omega(y,z)\} \tag{3}$$

The function Ω is an analytic function of the complex variable Z where

$$Z = y\sqrt{A} + iz \tag{4}$$

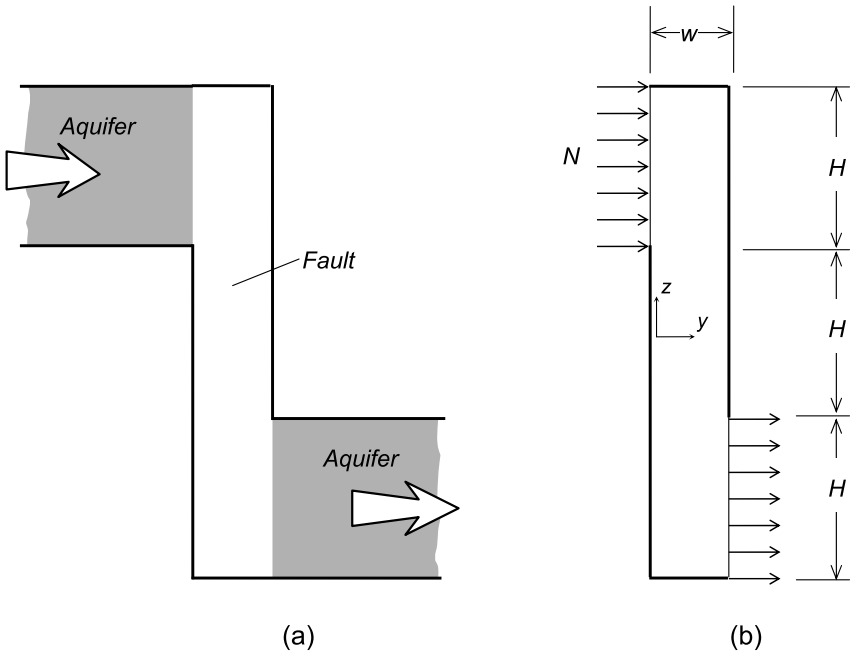

Figure 1. Definition sketch: (a) conceptual model of flow in an aquifer cut by a fault zone and (b) the idealized boundary value problem.

is a complex function of the physical coordinates, y and z. The function Ω is

$$\Omega = \frac{Nw\sqrt{A}}{\pi^2}\sum_{n=-\infty}^{n=+\infty}\mathrm{Li}_{2p}\left\{\exp\left[\frac{-i\pi}{w\sqrt{A}}\left(Z - i6nH - i\frac{H}{2}\right)\right]\right\} - \mathrm{Li}_{2p}\left\{\exp\left[\frac{-i\pi}{w\sqrt{A}}\left(Z - i6nH - i\frac{5H}{2}\right)\right]\right\} + \mathrm{Li}_{2p}\left\{-\exp\left[\frac{-i\pi}{w\sqrt{A}}\left(Z - w\sqrt{A} + i6nH + i\frac{H}{2}\right)\right]\right\} - \mathrm{Li}_{2p}\left\{-\exp\left[\frac{-i\pi}{w\sqrt{A}}\left(Z - w\sqrt{A} + i6nH + i\frac{5H}{2}\right)\right]\right\} + \Phi_o \quad (5)$$

The function $\mathrm{Li}_{2p}(z)$ is the principal branch of the dilogarithm of a complex variable [*Strack*, 1989], and Φ_o is a real constant evaluated from a reference point of known head.

[13] This solution was obtained by first solving the problem of a single recharge segment in an infinite, isotropic, vertical strip using conformal mapping and boundary integral methods; the derivation follows closely the work of *Anderson* [2003a]. The second recharge segment, opposite the fault from the first, is added by superposition of the same basic solution. The conditions along the top and bottom impermeable boundaries are satisfied by adding an infinite series of images of the two recharge segments, extending both up and down the infinite strip. Finally, the standard transformation [*Bear and Dagan*, 1965] from an isotropic domain to an anisotropic one is made. We chose an analytical rather than a numerical approach to solve this problem so that cases with large anisotropy ratios could be evaluated accurately without having to assess and adjust computational grids to obtain accurate results.

[14] Figure 2 shows flow nets obtained from (5) for increasing anisotropy ratio, A, ranging from 10^0 to 10^4. In each plot, the dashed lines are contours of hydraulic head and the solid lines are contours of the stream function. The contour interval is the same in all plots. The isotropic case is shown in Figure 2a; the closely spaced head contours indicate significant head loss due to vertical flow. That head loss is seen to be significantly decreased in Figure 2b where the anisotropy ratio has a value of 10. Figure 2c shows the case for an anisotropy ratio of 100; here the contours of head have become nearly vertical, and head loss due to vertical flow has become small in comparison to Figures 2a and 2b. In Figures 2d and 2e the anisotropy ratio is again increased by a factor of 10 for each case, and the head contours are almost indistinguishable from vertical. The effect of anisotropy on the streamlines in Figures 2d and 2e is profound. The streamlines jump vertically from their initial positions along the boundaries of the domain, while the flow is primarily horizontal throughout the rest of the domain. The limiting case of an infinite anisotropy ratio results in true Dupuit type flow within the fault [*Polubarinova-Kochina*, 1962; *Strack*, 1989]: the head does not vary vertically within the fault, and the flow is distributed uniformly in the vertical direction.

[15] The specific dimensions of the fault presented here were chosen to produce clear flow nets that can be interpreted visually. The solution was used to investigate other geometries, as well as multiaquifer flow to the fault. Multiaquifer flow was simulated by including multiple recharge strips of constant normal component of flow along the boundaries, using superposition of the basic solution (5). In all cases examined, the condition $A \geq 100$ produced nearly hydrostatic conditions in the fault. These results verify the hypothesis of *Bredehoeft et al.* [1992] that large vertical anistropy in fault zones can result in the nearly

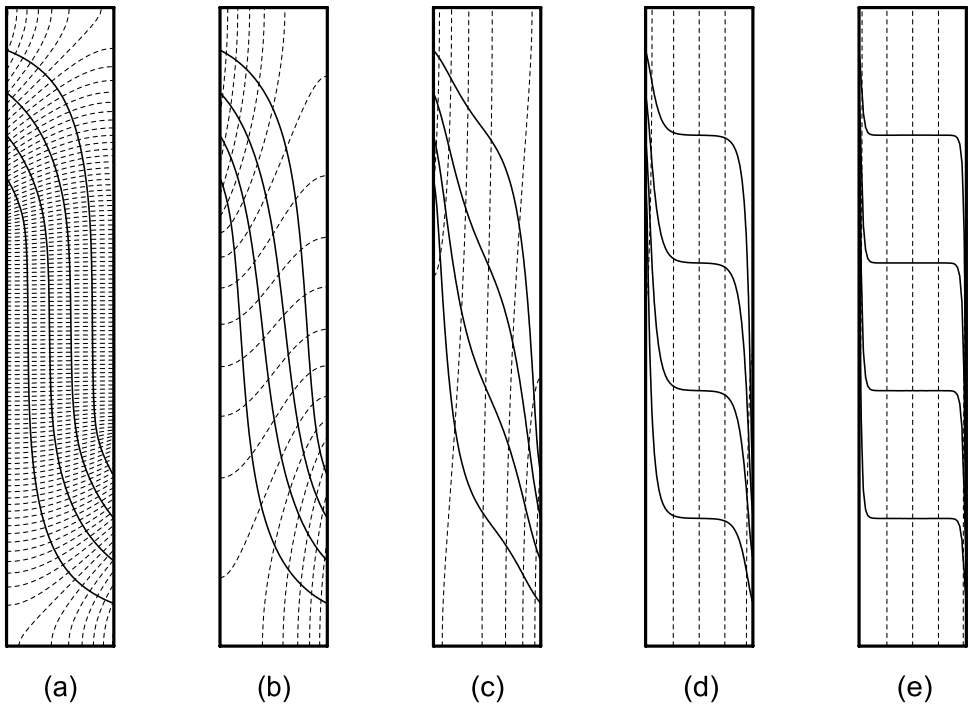

Figure 2. Flow nets for increasing anisotropy ratio, A: (a) $A = 1$, (b) $A = 10$, (c) $A = 100$, (d) $A = 1{,}000$, and (e) $A = 10{,}000$. Dashed lines are contours of hydraulic head ($\Delta h k_y/(wN) = 0.04$), and solid lines are contours of stream function ($\Delta\Psi/(NH) = 0.2$).

hydrostatic conditions observed in the Big Horn Basin. Further evidence of the effects of anisotropy on the head distribution within a fault is provided by *Bense and Person* [2006]. Figure 12g of that article shows a vertical fault, with $A = 10^3$, through a multiaquifer system; although the topic of nearly hydrostatic conditions is not discussed in the paper, close inspection of Figure 12g shows that the head contours in the fault zone are indeed nearly vertical. On the basis of our investigation and the findings of the cited references, we propose to adopt the Dupuit approximation to model flow within highly anisotropic fault zones.

3. Problem Description: A Faulted Multiaquifer System

[16] We next consider steady flow to a well screened in a single aquifer of a multiaquifer system, as illustrated in Figure 3. The system consists of N aquifer layers separated by $N - 1$ leaky layers. The well at coordinates (x_w, y_w) has a discharge Q and is located near an infinitely long geological fault that lies along the x axis. The well is located in domain D^- ($y < 0$) and in layer number p. Domain D^+ lies on the other side of the fault, where the properties of the aquifers and leaky layers, as well as the number of layers M, may be different from those in D^-; domains D^- and D^+ are semi-infinite. The Dupuit approximation is adopted within each aquifer layer, and the flow through the leaky layers is approximated as vertical.

[17] The aquifer properties in D^- are indicated with Greek symbols: τ_n represents the transmissivity of aquifer n ($n = 1, \ldots, N$), and ρ_n represents the resistance of leaky layer n ($n = 2, \ldots, N$). The properties in D^+ are indicated with Roman letters: T_m represents the transmissivity of aquifer m ($m = 1, \ldots, M$) and R_m represents the resistance of leaky layer m ($m = 2, \ldots, M$). Aquifer transmissivities are written as vectors $\vec{\tau}$ and $\vec{T}$. Unit transmissivity vectors, of which the components sum to one, are used for convenience: $\vec{\tau}_u = \vec{\tau}/\tau$ and $\vec{T}_u = \vec{T}/T$. The comprehensive transmissivities τ and T are equal to the sum of the transmissivities in all aquifers: $\tau = \sum \tau_n$ and $T = \sum T_m$.

[18] We showed in section 2 that large vertical anisotropy ratios, greater than 10^2, in the fault are approximated well by applying the Dupuit approximation within the fault. As a result, the head may vary tangentially to the fault in the horizontal plane, and may jump from one side of the fault to the other, but the head does not vary in the vertical direction. At a point $(x,0)$ along the fault in D^-, the heads are equal in all aquifers layers; at the same point $(x,0)$ in D^+, the head may differ from that in D^-, but again, the heads are equal in all aquifer layers. We will consider two fault types in detail, and will present their specific boundary conditions in the upcoming sections. First, we will present a general solution approach applicable to all fault types discussed in this paper.

4. Solution Approach

[19] We describe here the general solution for steady multiaquifer flow based on the work of *Hemker* [1984], *Maas* [1986], and *Bakker and Strack* [2003], and then present our solution approach that will be applied in the upcoming sections. Multiaquifer flow is formulated in terms of a vector of discharge potentials $\vec{\Phi}$ where component i is defined as

$$\begin{aligned} \Phi_i &= \tau_i h_i \qquad (i = 1, \ldots, N) \qquad \text{in} \quad D^- \\ \Phi_i &= T_i h_i \qquad (i = 1, \ldots, M) \qquad \text{in} \quad D^+ \end{aligned} \tag{6}$$

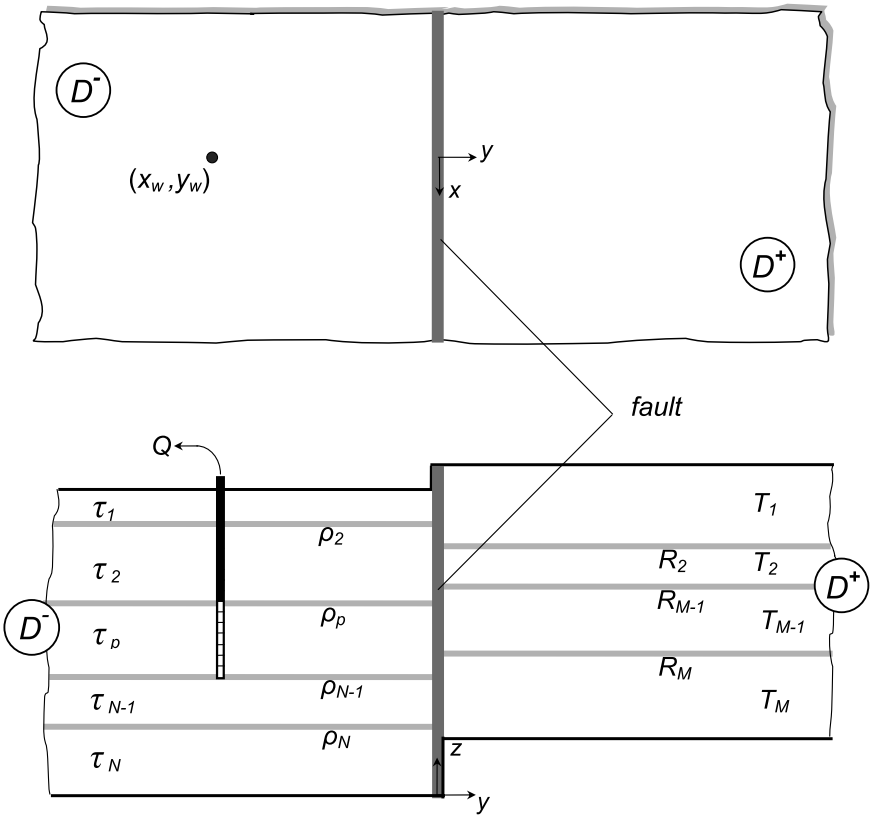

Figure 3. Definition sketch: flow to a pumping well near a fault in a multiaquifer system. The complex ζ plane (horizontal plane) and a section through the fault along the y axis (vertical plane) are illustrated.

and where h_i is the head in layer i. The x and y components of the discharge vector, the specific discharge vector integrated over the aquifer thickness, are each written as vectors as well, where component i is the discharge in aquifer i. The components of the discharge vector may be obtained from the potential as

$$\vec{Q}_x = -\frac{\partial \vec{\Phi}}{\partial x} \qquad \vec{Q}_y = -\frac{\partial \vec{\Phi}}{\partial y} \tag{7}$$

For steady flow, $\vec{\Phi}$ satisfies the following system of differential equations

$$\nabla^2 \vec{\Phi} = \mathbf{A}\vec{\Phi} \tag{8}$$

The system matrix $\mathbf{A}$ is a tridiagonal matrix, with diagonal terms defined in D^- as

$$A_{n,n} = \frac{1}{\rho_n \tau_n} + \frac{1}{\rho_{n+1}\tau_n} \tag{9}$$

and with off-diagonal terms

$$A_{n,n-1} = \frac{-1}{\rho_n \tau_{n-1}}, \qquad A_{n,n+1} = \frac{-1}{\rho_{n+1}\tau_{n+1}} \tag{10}$$

where it is used that $\rho_1 = \rho_{N+1} = \infty$ to represent an impermeable aquifer top and bottom. $\vec{\Phi}$ fulfills the same system of differential equations in D^+, but in the definition of $\mathbf{A}$, the parameters ρ and τ are replaced with R and T, respectively, and the number of layers N is replaced with M.

[20] The general solution to the system of coupled differential equations in D^- (8) may be written as

$$\vec{\Phi} = \Phi\vec{\tau}_u + \sum_{n=1}^{N-1} F_n \vec{\nu}_n \qquad \text{in} \quad D^- \tag{11}$$

where Φ (no vector arrow on top, no index below) is the comprehensive potential, which fulfills Laplace's equation, and F_n fulfills the modified Helmholtz equation

$$\nabla^2 F_n = F_n/\lambda_n^2 \tag{12}$$

where $\lambda_n = 1/\sqrt{\omega_n}$ is leakage factor n, ω_n is eigenvalue n of system matrix $\mathbf{A}$, and $\vec{\nu}_n$ is the corresponding eigenvector. We note that the first term in (11) corresponds to an eigenvalue of zero [e.g., *Bakker and Strack*, 2003]. The comprehensive potential, Φ, is the sum of the potentials of all the aquifers. The term $\Phi\vec{\tau}_u$ by itself results in a head h that does not differ between aquifers

$$\Phi\vec{\tau}_u = h\vec{\tau} \tag{13}$$

where $h = \Phi/\tau$ is the comprehensive head corresponding to the comprehensive potential.

[21] The form of the general solution to (8) in D^+ is similar to (11), except that the heads do not differ between aquifers in D^+. This is explained as follows: Domain D^+ is

bounded along the x axis by the fault and the head along the fault does not vary in the vertical direction; as there are no other features in D^+ causing a head difference between aquifers, the heads are the same in all aquifers and all functions F_n in (11) are zero, so that

$$\vec{\Phi} = \Phi \vec{T}_u \qquad \text{in} \quad D^+ \tag{14}$$

A solution to a given problem is complete when the expressions for the comprehensive potential Φ in both D^- and D^+ and the functions F_n in D^- have been obtained.

[22] As stated, we will consider a well pumping in layer p near different types of faults. The well has discharge Q and is located at (x_w, y_w) in D^-. For each fault type, the equivalent single-aquifer solution is presented in *Anderson* [2006]. The single-aquifer solution is the comprehensive potential in (11) and (14). The comprehensive potential fulfills all boundary conditions along the fault (recall that the heads do not vary in the vertical direction along the fault). The comprehensive potential satisfies the following boundary condition at the well:

$$\lim_{r \to 0} \left[2\pi r \frac{\partial \Phi}{\partial r} \right] = Q \tag{15}$$

where $r = \sqrt{(x - x_w)^2 + (y - y_w)^2}$, and the partial derivative may be evaluated at any θ. The first term in the solution in D^- (11) now satisfies the following condition:

$$\lim_{r \to 0} \left[2\pi r \frac{\partial \Phi}{\partial r} \vec{\tau}_u \right] = Q \vec{\tau}_u \tag{16}$$

Hence, the term $\Phi \vec{\tau}_u$ represents a well of which the discharge in layer n is $Q\tau_n/\tau$. To obtain the solution for a well with a discharge Q in pumping layer p and a zero discharge in the other layers, we need to add the solution for a multiaquifer well with a discharge $-Q\tau_n/\tau$ in every layer but p, and a discharge $Q - Q\tau_p/\tau$ in layer p. The general solution for a multiaquifer well with a zero total discharge is obtained from *Bakker and Strack* [2003] and has the form

$$\vec{\Phi} = \sum_{n=1}^{N-1} \frac{\alpha_n}{2\pi} \mathrm{K}_0(r/\lambda_n) \tag{17}$$

where α_n are constants. To maintain the correct behavior along the fault, the head and thus the potential must vanish along the fault. A zero head along the fault is obtained by adding another multiaquifer well imaged about the fault. The functions F_n may now be written as

$$F_n = \frac{\alpha_n}{2\pi} [\mathrm{K}_0(r/\lambda_n) - \mathrm{K}_0(\bar{r}/\lambda_n)] \tag{18}$$

where the radial coordinate $\bar{r}$ originates from the image well: $\bar{r} = \sqrt{(x - x_w)^2 + (y + y_w)^2}$. The $N - 1$ coefficients α_n are obtained from the following set of linear equations [*Bakker and Strack*, 2003, equation 11],

$$\sum_{j=1}^{N-1} \alpha_j \nu_{j,n} = Q\tau_n/\tau, \qquad n = 1, \ldots, N; \quad n \neq p \tag{19}$$

where $\nu_{j,n}$ is component n of eigenvector $\vec{v}_j$. This linear system may be solved by a standard method. The general solution for a well in a multiaquifer system pumping near a fault with a high vertical conductivity is complete. The solution is given by (11) and (14), where the comprehensive potential is obtained from the equivalent single-aquifer problem given in *Anderson* [2006], and the functions F_n are given in (18). Note that the functions F_n are the same for all types of faults considered here. Analytic derivatives of the functions F_n, needed for the computation of pathlines, are given by *Bakker* [2001, equation 16]. In the remainder of this paper, we will consider in detail two types of faults, defined by the comprehensive potential.

5. A Well Near a Leaky Fault

[23] We first consider a well near a leaky fault. The horizontal component of the transmissivity tensor normal to a leaky fault is small compared to the comprehensive transmissivities of the aquifer systems on either side of the fault; the horizontal component of the transmissivity tensor tangential to a leaky fault is zero ($k_x = 0$) [*Anderson*, 2003b]. We represent the properties of the fault as a resistance to normal flow, R_f (T/L), and treat the fault as an internal boundary condition [*Anderson*, 2006]. This type of fault is often described as a barrier to groundwater flow. The resistance of the fault, R_f, is defined as the ratio of the fault width to the normal transmissivity of the fault

$$R_f = w/(k_y H_f) \tag{20}$$

where H_f is the depth of the fault zone. The flow across the fault depends on the head difference across the fault and the resistance, R_f

$$Q_y^- = Q_y^+ = \frac{h^- - h^+}{R_f} = \frac{1}{R_f} \left[\frac{\Phi^-}{\tau} - \frac{\Phi^+}{T} \right] \qquad \text{for} \quad (x, 0) \tag{21}$$

where Q_y (no vector arrow on top) is the y component of the comprehensive discharge vector, the discharge summed over all aquifers.

[24] The comprehensive potential, satisfying Laplace's differential equation and the boundary conditions (21), is written as the real part of a complex potential $\Omega = \Phi + i\Psi$ of the complex variable $\zeta = x + iy$, where Ψ is the stream function. The well is located at the complex coordinate $\zeta_w = x_w + iy_w$. The comprehensive potential, or the single-aquifer solution, is given by *Anderson* [2006] and rewritten here as

$$\Omega = \frac{Q}{2\pi} \ln(\zeta - \zeta_w) + \frac{Q}{2\pi} \left(\frac{\tau - T}{\tau + T} \right) \ln(\zeta - \overline{\zeta_w}) + B \exp(\zeta_1) \mathrm{E}_1(\zeta_1) + C, \qquad \zeta \quad \text{in} \quad D^- \tag{22}$$

$$\Omega = \frac{Q}{\pi} \left(\frac{T}{\tau + T} \right) [\ln(\zeta - \zeta_w) + \exp(\zeta_2) \mathrm{E}_1(\zeta_2)] + \frac{T}{\tau} C, \qquad \zeta \quad \text{in} \quad D^+ \tag{23}$$

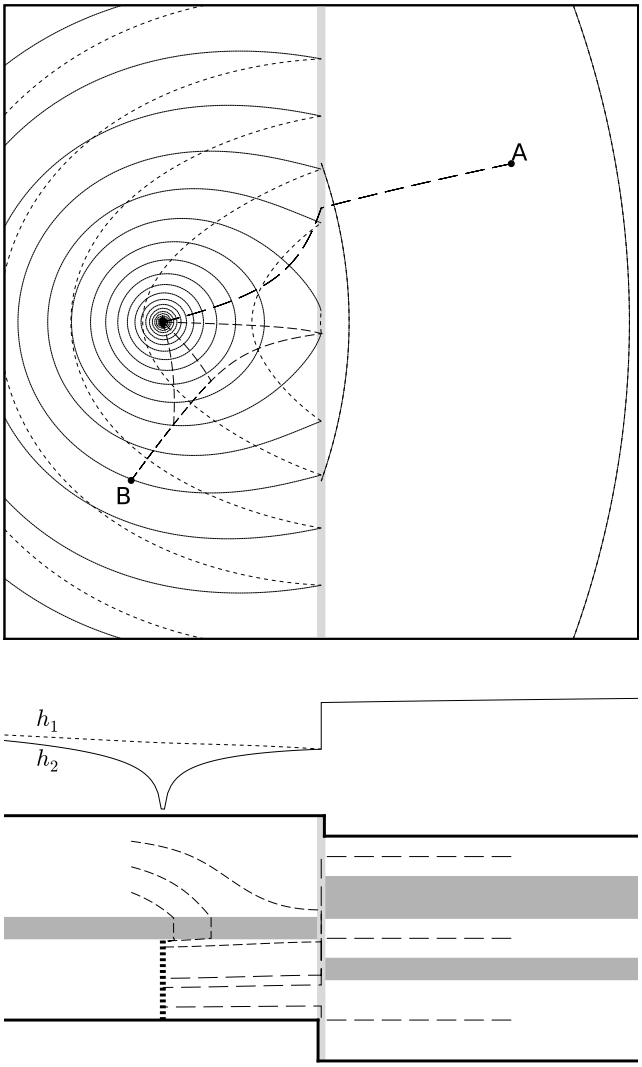

Figure 4. (top) Plan view and (bottom) cross-sectional view in the plane normal to the fault and through the well for example of a well pumping near a leaky fault (light grey). Plan view includes contours of head (contour interval 2 cm), small dashes are contours in top aquifer on side of well, and solid lines are contours of head in all other aquifers. Cross-sectional view includes heads in cross section and location of leaky layers (dark grey). Pathlines starting at point *A* (long dash) and *B* (medium dash) are shown in both the plan view and as a projection on the cross-sectional view.

where

$$B = -\frac{Q}{\pi}\left(\frac{T}{\tau + T}\right) \tag{24}$$

$$\zeta_1 = \frac{i}{R_f}\left(\frac{\tau + T}{\tau T}\right)\left(\zeta - \overline{\zeta_w}\right) \tag{25}$$

$$\zeta_2 = -\frac{i}{R_f}\left(\frac{\tau + T}{\tau T}\right)(\zeta - \zeta_w) \tag{26}$$

and where C is a real constant that may be evaluated from the head at a reference point. The comprehensive discharge vector may be obtained from differentiation of the comprehensive discharge potential and is presented by *Anderson* [2006].

6. Example of a Well Near a Leaky Fault

[25] As an example, we consider a well pumping in the lower aquifer of a two-aquifer system near a leaky fault. On the side of the fault opposite the well the system consists of three aquifers. Aquifer properties on the side of the well are $\tau_1 = 100$, $\tau_2 = 200$ m^2/d, and $\rho_2 = 250$ days. On the other side the properties are $T_1 = 20$, $T_2 = 50$, and $T_3 = 100$ m^2/d, and $R_2 = 500$ days and $R_3 = 2000$ days. The resistance of the fault is $R_f = 10$ d/m, which is equivalent to a fault with an effective horizontal transmissivity normal to the fault of 0.5 m^2/d and a width of 5 m. A well with a discharge of $Q = 100$ m^3/d is located a distance of 100 m from the well.

[26] A plan view of the aquifer system is presented in Figure 4 (top), where contours of the head are shown. A vertical cross section along a plane normal to the fault and through the well is shown in Figure 4 (bottom). The fault is indicated by the light grey line, although we emphasize that the fault is treated as a line of zero width in our solution. The dark grey zones in the cross section represent the leaky layers. Note that the aquifers are offset vertically by the fault; both the top and bottom of the aquifer system are higher on the side of the well than on the opposite side.

[27] In the plan view, the short dashes represent head contours in the top aquifer on the side of the well, while the solid lines represent head contours in the lower aquifer. Note that the heads in both aquifers are the same at the fault. On the side of the fault opposite the well, the heads are the same in all three aquifers and are represented by solid lines. The heads in the cross section are also shown, where the short dashes represent the head in the top aquifer (h_1) and the solid line the head in the bottom aquifer (h_2). In both the plan view and the cross-sectional view the jump in head across the fault is clearly visible. Also note that the y component of the flow in the top aquifer on the side of the well is always toward the fault and that the lowest head in the top aquifer occurs at the fault (at the origin of the coordinate system).

[28] Three pathlines begin at point A, one at the center of each aquifer. Each is shown on both the plan view and the cross-sectional view (long dashes). On the side opposite the well, the pathlines follow the same horizontal paths until they reach the fault, where they jump vertically into the aquifer where the well is screened. In this aquifer they again follow the same horizontal paths and they drift slightly down because of the leakage from the top aquifer.

[29] Three pathlines, indicated with medium-length dashes, begin at point B at three different elevations in the top aquifer. Initially they follow the same horizontal paths until the pathline with the lowest starting elevation passes through the leaky layer to the bottom aquifer where it extends to the well. The pathline with the second lowest starting elevation stays in the top aquifer for a longer distance, before is passes to the bottom aquifer through the leaky layer. The pathline with the highest starting elevation extends all the way to the fault where it jumps vertically down into the bottom aquifer from where it extends to the well. Note that this latter pathline is horizontal just before it enters the fault; at that point the heads in

the two aquifers are equal, and there is no vertical flow through the leaky layer.

[30] A final remark concerns the computation of the jump in elevation when pathlines starting at point A cross the fault. The new elevation of the pathline is computed by requiring that the comprehensive normal discharge below the pathline when it enters the fault is the same as the comprehensive normal discharge below the pathline when it exits the fault. This procedure is similar to that employed by *Strack* [1995] for the computation of pathlines in variable density flow in piecewise homogeneous aquifers; this procedure was validated against a three-dimensional solution by *Strack and Bakker* [1995].

7. A Well Near a Conductive Fault

[31] *Anderson* [2006] describes fault types affecting horizontal groundwater flow other than the leaky fault. The conductive fault has no fault resistance ($R_f = 0$) and the tangential fault transmissivity is represented by the conductance of the fault, C_f [L^3/T]

$$C_f = wk_xH_f \tag{27}$$

where w and H_f are the width and depth of the fault zone, respectively, and k_x is the horizontal component of the hydraulic conductivity tangential to the fault. The conductive fault is commonly referred to as a conduit for horizontal flow.

[32] The conductive fault is represented by the following conditions along the fault

$$\frac{\Phi^-}{\tau} = \frac{\Phi^+}{T} \tag{28}$$

$$C_f \frac{Q_x^-}{\tau} = C_f \frac{Q_x^+}{T} = \Psi^- - \Psi^+ \tag{29}$$

where Ψ^- and Ψ^+ are the complex conjugate functions of the comprehensive potential, Φ, on either side of the fault: Ψ is a stream function for the comprehensive potential. The first condition ensures that the head is continuous across the fault and the second ensures that the flow within the fault is equal to the jump in the stream function across the fault.

[33] For a well of strength Q at $\zeta = \zeta_w$ and lying in D^- the complex potential that satisfies conditions (28) and (29) is given by (22) and (23) with the parameters B, ζ_1, and ζ_2 defined for a conductive fault as

$$B = \frac{Q}{\pi}\left(\frac{\tau}{\tau + T}\right) \tag{30}$$

$$\zeta_1 = \frac{i}{C_f}(\tau + T)\left(\zeta - \overline{\zeta_w}\right) \tag{31}$$

$$\zeta_2 = -\frac{i}{C_f}(\tau + T)(\zeta - \zeta_w) \tag{32}$$

8. Example of a Well Near a Conductive Fault

[34] We consider the same situation as in the example of a well near a leaky fault (section 6), but now the leaky fault is replaced by a conductive fault with a conductance C_f = 425,000 m^3/d. This conductance represents a fault with a width of 5 m and a transmissivity tangential to the fault of 8500 m^2/d. This value was chosen such that the resistance R_f used in the example of the leaky fault and the conductance used here fulfill the condition $C_f = \tau TR_f$, which results in a head distribution on the side of the fault opposite from the well that is exactly the same as for the example of the leaky fault [*Anderson*, 2006, equation 48].

[35] Results are shown in the plan view (top) and cross-sectional view (bottom) of Figure 5; line styles are equivalent to those used in Figure 4. Note that there is no jump in head across the fault in Figure 5, and that the head contours are indeed exactly the same on the side of the fault opposite the well in Figures 4 and 5. The minimum head in the top aquifer occurs to the left of the well, as indicated in the cross-sectional view. Three pathlines begin at point A at the center of each of the aquifers. All three pathlines follow the same horizontal paths until they reach the conductive fault. The pathlines enter the conductive fault and exit again near the well. The topmost pathline exits the fault in the top aquifer above the well and eventually passes to the bottom aquifer through the leaky layer where it continues to the well. The lower two pathlines exit the fault in the lower aquifer and extend directly to the well. Three pathlines also begin in the top aquifer at point B; the location of point B is chosen differently than in Figure 4, because the flow field is different. All three pathlines pass through the leaky layer to the bottom aquifer at different spots, from where they follow different paths to the well.

[36] The computation of the pathline through the fault is as follows. The horizontal location of the exit point of a pathline started at point A is computed by requiring that the entrance and exit points have the same value of the comprehensive stream function Ψ. Computation of the jump in elevation of a pathline crossing the fault is slightly different from the leaky fault, because the normal component of the comprehensive discharge differs between the entrance and exit points. The fraction of the comprehensive normal discharge below the pathline is computed at the entrance point. The elevation of the exit point is computed by requiring that the fraction of the comprehensive normal discharge below the pathline at the exit point is the same as at the entrance point.

[37] Variations in the parameter values may change the characteristics of the flow field. We evaluate the effects of the conductivity of the fault and of the resistance of the leaky layer above the well. The setup of Figure 5 is used as the base case and we vary only one parameter at a time. The results are shown in Figure 6; only the plan view is shown, the contour interval is the same for all plots, and only one pathline begins at point A (at the center of the middle aquifer) and at point B (at the center of the top aquifer). In Figure 6a, we increase the conductance by a factor of 10. This larger value results in an almost constant head along the fault (no head contours exist within the contour interval used) and almost no flow on the side of the fault opposite the well. The pathline from point A extends almost all the way to the origin through the fault, and from there to the well. The minimum head in the top aquifer on the side of the well has shifted significantly to the left. In Figure 6b we decrease the conductance of the fault by a factor of 10. This

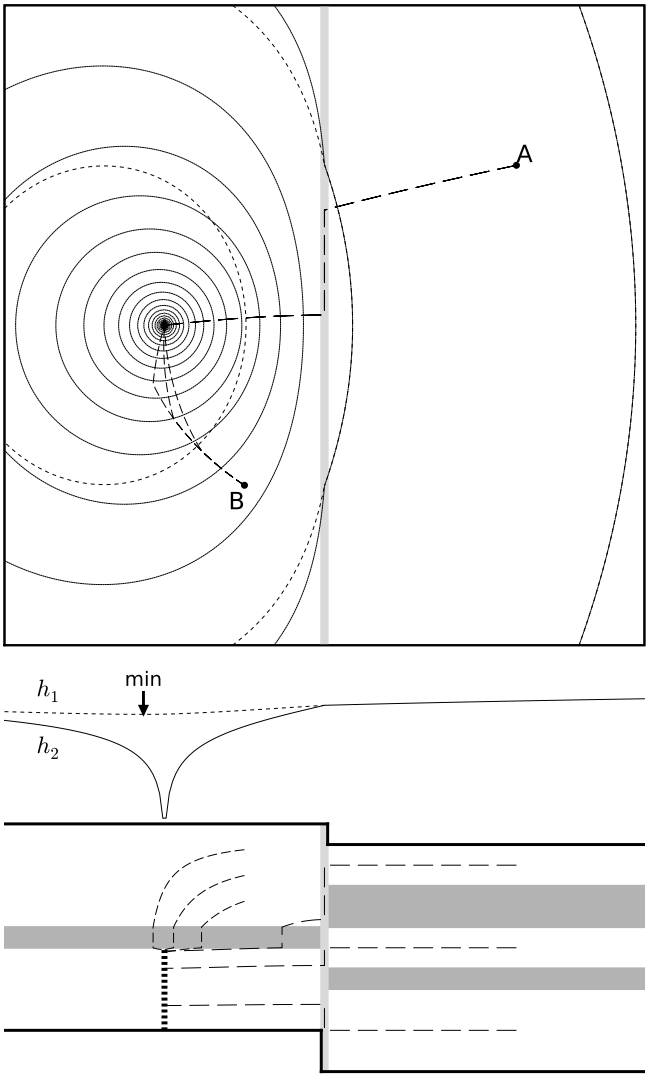

Figure 5. (top) Plan view and (bottom) cross-sectional view in the plane normal to the fault and through the well for example of a well pumping near a conductive fault (light grey). Plan view includes contours of head (contour interval 2 cm), small dashes are contours in top aquifer on side of well, and solid lines are contours of head in all other aquifers. Cross-sectional view includes heads in cross section and location of leaky layers (dark grey). Pathlines starting at point *A* (long dash) and *B* (medium dash) are shown in both the plan view and as a projection on the cross-sectional view.

causes a larger head gradient along the fault, and thus a more significant amount of flow on the side of the fault opposite the well. The pathline that begins at point A now passes only a small distance within the fault before it extends to the well. The minimum head in the top aquifer on the side of the well has shifted to a point slightly to the right of the well. In Figures 6c and 6d, the conductance of the fault is set to its original value and the resistance of the leaky layer above the well is either increased by a factor of 10 (Figure 6c) or decreased by a factor of 10 (Figure 6d). In either case, there is no effect on the heads on the side of the fault opposite the well, where they are the same as in Figure 5. The heads in the aquifer above the well change, of course. With an increased resistance (Figure 6c) there is little flow in the aquifer above the well. The minimum head is at the fault, and the pathline starting at point B extends to the fault, where it passes down to the bottom aquifer and then to the well. With a smaller resistance (Figure 6d) the head contours in the aquifer above the well resemble the head contours in the aquifer with the well. The pathline starting at point B extends almost directly toward the well and passes down to the bottom aquifer at approximately two thirds of the total distance to the well.

9. Extensions of the Analytical Model

[38] The analytical model presented here is quite flexible and can be modified to represent a fault with more general properties, as well as including more complex aquifer flow features.

[39] The final fault type discussed by *Anderson* [2006] is the general fault, which includes both nonzero resistance and nonzero conductance. The solution for a well pumping near a general fault in a multiaquifer system may be obtained, as for the previous fault solutions, by specifying the comprehensive potential to be the single-aquifer solution presented by *Anderson* [2006, equation 21]. This solution represents the fault as having a three-dimensional anisotropy where the vertical fault conductivity is infinite, or very large compared to the other components. Examples of the general fault in a single aquifer are presented by *Anderson* [2006].

[40] The presented solutions allow for the horizontal properties of the fault (C_f and R_f) to vary over the depth of the fault by redefining those properties as depth-integrated values [*Strack*, 1989, pp. 113–115]. In this manner use can be made of the shale gouge ratio [*Harris et al.*, 2002] or similar heuristics [*Bense and Person*, 2006] that predict changes in fault zone permeability and width over the depth of the fault.

[41] The multiaquifer solution of *Maas* [2000] may be obtained as a special case of either the leaky or conductive fault solutions, simply by specifying $R_f = 0$ for the former solution, or $C_f = 0$ in the latter solution. The solution of *Hunt and Curtis* [1989] may also be obtained as a special case in the same manner by specifying, in addition, $\tau = T$ and setting the number of aquifers on the side of the fault opposite the well to $M = 1$.

[42] The analytical framework we have presented is flexible enough to be extended, through superposition, to include many other flow features. Simple examples include multiple pumping wells in any aquifer and on either or both sides of the fault, a uniform flow in the far field oriented at any direction, one-dimensional recharge oriented normal to the fault, and localized recharge from circular ponds. Further, the analytic element method may be used to represent other aquifer features approximately, while maintaining the conditions along the fault exactly. These features include canals, streams, and inhomogeneities. The comprehensive potential for these features may be developed using line elements and their images about the fault, presented in *Anderson* [2000a, 2000b]; the multiaquifer component of the solution is obtained by the imaging described here using elements developed by *Bakker and Strack* [2003].

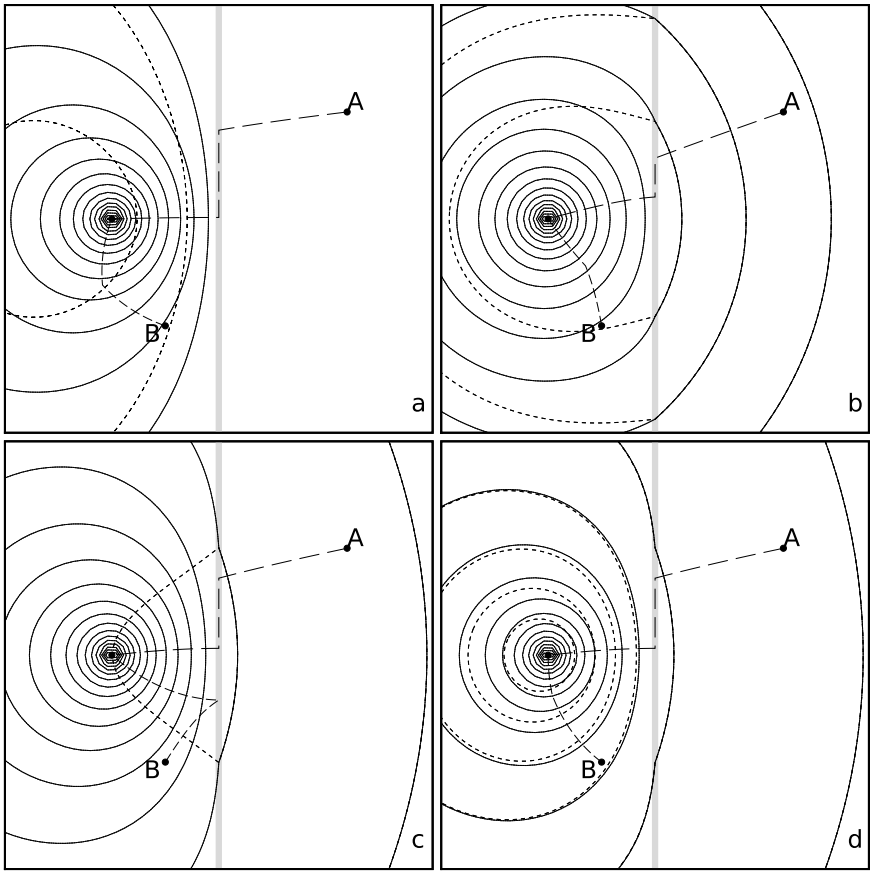

Figure 6. Results after varying the problem parameters: (a) fault conductance increased by a factor of 10, (b) fault conductance decreased by a factor of 10, (c) resistance of the leaky layer above the well increased by a factor of 10, and (d) resistance of the leaky layer decreased by a factor of 10.

[43] The multiaquifer solutions and examples presented here were implemented and tested using the open source analytic element software *Tim*^{ML} (M. Bakker, *Tim*^{ML} A multiaquifer analytic element model, version 3, 16 February 2007, available at http://www.bakkerhydro.org). A more general, but approximate, framework for modeling faults in multiaquifer systems may be developed using the same software. This framework would allow the faults to be finite in length and piecewise linear in the horizontal plane, and incorporate a vertical resistance to flow within the fault. The boundary conditions along the fault would be met approximately, but very accurately using analytic elements.

10. Discussion and Conclusions

[44] We have evaluated the effects of vertical anisotropy on flow within a fault in a rigorous way by incorporating anisotropy into an analytical solution, and have explained the field observations and numerical results of *Bredehoeft et al.* [1992] indicating nearly hydrostatic conditions in highly anisotropic, multiaquifer faults. We have placed a lower bound of 100 on the vertical anisotropy ratio within a fault required to produce nearly hydrostatic conditions, and have shown by reference that this value of the anisotropy ratio is commonly believed to exist in many faults in a variety of geologic settings.

[45] Our results indicate that the Dupuit approximation may be used to model accurately the flow of groundwater within highly anisotropic faults. Adoption of the Dupuit approximation within the fault leads to a significant simplification of the mathematical problem, and allows for a fully analytical solution for the complex three-dimensional flow within and near faults in multiaquifer systems. A general solution was presented consisting of two terms: the first term represents a comprehensive potential which meets the complicated boundary conditions along a fault; the second term represents leakage between aquifers without disturbing the boundary conditions along the fault.

[46] Our analytical solution is more general in the representation of fault properties than the numerical models of *Bredehoeft et al.* [1992] and *Bense and Person* [2006], both of which consider only the effects of leaky faults with enhanced vertical conductivity. Our model includes three-dimensional anisotropy of the fault, allowing for nonzero conductance and nonzero resistance in the horizontal plane, and enhanced vertical conductivity. The analytical solution also includes more general flow features in the aquifer by considering the effects of wells on the flow field. It is possible to use the analytical model with discharge and recharge wells to design steady state pumping tests to help identify fault properties.

[47] We have presented examples and results for a well pumping near both a leaky fault and a conductive fault in a multiaquifer system, and have demonstrated the intricacies in the head distribution in the aquifers and the three-

dimensional pathlines through the fault zone. We showed that for a well pumping near a multiaquifer fault, identical head patterns may be obtained on the side of the fault opposite from the well by choosing the values of R_f and C_f appropriately; this feature was discovered for single-aquifer faults by *Anderson* [2006]. Although the conductive fault has been discussed in the literature, we have found no other analytical or numerical investigations of the effects of a horizontally conductive fault on the flow field in a multi-aquifer system. A brief parametric study was conducted for the example of the conductive fault, showing the effects of variation of the problem parameters on the head distribution and pathlines to the well.

References

Anderson, E. I. (2000a), The method of images for leaky boundaries, *Adv. Water Resour.*, *23*, 461–474.

Anderson, E. I. (2000b), The method of images for leaky boundaries, paper presented at 3rd International Conference on the Analytic Element Method in Modeling Groundwater Flow, U.S. Environ. Prot. Agency, Brainerd, Minn., 16–19 April.

Anderson, E. I. (2003a), An analytical solution representing groundwater-surface water interaction, *Water Resour. Res.*, *39*(3), 1071, doi:10.1029/2002WR001536.

Anderson, E. I. (2003b), An approximation for leaky boundaries in groundwater flow, *J. Hydrol.*, *274*(1–4), 160–175.

Anderson, E. I. (2006), Analytical solutions for flow to a well through a fault, *Adv. Water Resour.*, *29*, 1790–1803.

Antonellini, M., and A. Aydin (1994), Effect of faulting on fluid flow in porous sandstones: Petrophysical properties, *AAPG Bull.*, *78*, 355–377.

Bakker, M. (2001), An analytic, approximate method for modeling steady, three-dimensional flow to partially penetrating wells, *Water Resour. Res.*, *37*(5), 1301–1308.

Bakker, M. (2006), Analytic element modeling of embedded multi-aquifer domains, *Ground Water*, *44*(1), 81–85.

Bakker, M., and O. D. L. Strack (2003), Analytic elements for multiaquifer flow, *J. Hydrol.*, *271*(1–4), 119–129.

Bakker, M., E. I. Anderson, T. N. Olsthoorn, and O. D. L. Strack (1999), Regional groundwater modeling of the Yucca Mountain site using analytic elements, *J. Hydrol.*, *258*(1–4), 167–178.

Bear, J., and G. Dagan (1965), The relationship between solutions of flow problems in isotropic and anisotropic soils, *J. Hydrol.*, *3*, 88–96.

Bense, V. F., and M. A. Person (2006), Faults as conduit-barrier systems to fluid flow in siliciclastic sedimentary aquifers, *Water Resour. Res.*, *42*, W05421, doi:10.1029/2005WR004480.

Bense, V. F., R. T. van Balen, and J. J. de Vries (2003a), The impact of faults on the hydrogeological coditions in the Roer Valley Rift System: An overview, *Neth. J. Geosci.*, *82*(1), 317–320.

Bense, V. F., E. H. van den Berg, and R. T. van Balen (2003b), Deformation mechanisms and hydraulic properties of fault zones in unconsolidated sediments: The Roer Valley Rift System, the Netherlands, *Hydrogeol. J.*, *11*(3), 319–332.

Bredehoeft, J. D., K. Belitz, and S. Sharp-Hansen (1992), The hydrodynamics of the Big Horn Basin: A study of the role of faults, *AAPG Bull.*, *76*(1), 530–546.

Caine, J. S., and C. B. Forester (1999), Fault zone architecture and fluid flow: Insights from field data and numerical modeling, in *Faults and Subsurface Fluid Flow in the Shallow Crust*, *Geophys. Monogr. Ser.*, vol. 113, edited by W. C. Haneberg et al., pp. 101–127, AGU, Washington, D. C.

Flodin, E. A., L. J. Durlofsky, and A. Aydin (2004), Upscaled models of flow and transport in faulted sandstone: Boundary condition effects and explicit fracture modelling, *Pet. Geosci.*, *10*, 173–181.

Harris, D., G. Yielding, P. Levine, G. Maxwell, P. T. Rose, and P. Nell (2002), Using shale gouge ratio (SGR) to model faults as transmissibility barriers in reservoirs: An example from the Strathspey Field, North Sea, *Pet. Geosci.*, *8*, 167–176.

Hemker, C. J. (1984), Steady groundwater flow in leaky multiple-aquifer systems, *J. Hydrol.*, *72*, 355–374.

Hunt, B., and T. G. Curtis (1989), Flow to a well near a boundary between a layered and an unlayered aquifer system, *Water Resour. Res.*, *25*(3), 559–563.

Jourde, H., E. A. Flodin, A. Aydin, L. J. Durlofsky, and X. H. Wen (2002), Computing permeability of fault zones in eolian sandstone from outcrop measurements, *AAPG Bull.*, *86*(7), 1187–1200.

Maas, C. (1986), The use of matrix differential calculus in problems of multiple-aquifer flow, *J. Hydrol.*, *88*, 43–67.

Maas, C. (2000), Drawdown pattern due to a well near a geological fault, paper presented at 3rd International Conference on the Analytic Element Method in Modeling Groundwater Flow, U.S. Environ. Prot. Agency, Brainerd, Minn., 16–19 April.

Maslia, M. L., and D. C. Prowell (1990), Effect of faults on fluid flow and chloride contamination in a carbonate aquifer system, *J. Hydrol.*, *115*, 1–49.

Polubarinova-Kochina, P. Y. (1962), *Theory of Ground Water Movement*, translated by J. M. R. DeWiest, Princeton Univ. Press, Princeton, N. J.

Strack, O. D. L. (1989), *Groundwater Mechanics*, Prentice Hall, Englewood Cliffs, N. J.

Strack, O. D. L. (1995), A Dupuit-Forchheimer model for three-dimensional flow with variable density, *Water Resour. Res.*, *31*(12), 3007–3017.

Strack, O. D. L., and M. Bakker (1995), A validation of a Dupuit-Forchheimer formulation for flow with variable density, *Water Resour. Res.*, *31*(12), 3019–3024.

E. I. Anderson, SEH Inc., 425 West Water Street, Suite 300, Appleton, WI 54911-6058, USA. (erik.isaac.anderson@gmail.com)

M. Bakker, Water Resources Section, Faculty of Civil Engineering and Geosciences, Delft University of Technology, NL-2628 CN Delft, Netherlands. (markbak@gmail.com)